Shape of Space Debris as Estimated from Radar Cross Section Variations

T. Sato, T. Wakayama, T. Tanaka,
K.-i. Ikeda, I. Kimura

Reprinted from

Journal of Spacecraft and Rockets

Volume 31, Number 4, Pages 665–670

A publication of the
American Institute of Aeronautics and Astronautics, Inc.
370 L'Enfant Promenade, SW
Washington, DC 20024-2518

JOURNAL OF SPACECRAFT AND ROCKETS
Vol. 31, No. 4, July–August 1994

Shape of Space Debris as Estimated from Radar Cross Section Variations

Toru Sato,* Toshio Wakayama,† and Takeshi Tanaka†
Kyoto University, Kyoto 606-01, Japan
Ken-ichiro Ikeda‡
University of Tokyo, Bunkyo-ku, Tokyo 113, Japan
and
Iwane Kimura§
Kyoto University, Kyoto 606-01, Japan

A special observation mode for space debris was developed for a vhf phased-array radar to measure the time variation of the radar cross section (RCS). Since a simple low-frequency approximation holds for the analysis of scattering of the radar signal from most of space debris, it is feasible to estimate the effective axial ratio of each target from the magnitude of the observed RCS variations. Preliminary statistical study showed that debris with smaller RCS has larger RCS variations than larger debris, suggesting that they may have elongated shape rather than spherical shape as usually assumed in the impact estimation. A series of numerical simulations has shown that the volume of small observed debris is estimated to be less than half of that of a sphere with the same RCS.

Nomenclature

$A(\theta, \phi)$	=	projected surface area as a function of polar angle θ and azimuthal angle ϕ, m^2
A_{eff}	=	average projected surface area of an object perpendicular to the direction of motion, m^2
a, b, c	=	length of the three axes of an ellipsoid in ascending order, m
b_e, c_e	=	geometrical mean distance of a cross section a-b and a-c, respectively
C	=	outer boundary of a cross section
d	=	distance between two points on C, m
$E(x)$	=	complete elliptic integral of the second kind
l	=	length of the outer boundary C, m
r	=	geometrical mean distance of a cross section, m
S	=	mean value of the RCS, m^2
η, ξ	=	coordinate along the outer boundary C of the cross section, m

Introduction

RADAR observation is the most practical way of studying the space debris environment on the low-Earth orbit as far as the objects of larger than 1 cm are concerned.[1]

The middle and upper atmosphere (MU) radar of Japan has the lowest frequency (46.5 MHz) among all radars used for debris observation. Since the radar backscattering cross section (RCS) is proportional to the sixth power of size for objects smaller than the radar wavelength, it is disadvantageous to employ a wavelength as large as 6.4 m in detecting small objects. However, the reduced RCS of small debris is compensated for by the large antenna aperture and the high output power, and thus the radar has shown comparable sensitivity in space debris detection to those employed by US SPACECOM for routine monitoring of space debris.[2] Figure 1 compares the height distribution of space debris observed by the MU radar with that determined from the US SPACECOM catalog. The radar data is that taken during 1989, and the catalog is as of July 1989.

Determination of the relation between RCS and its shape and mass is one of the most important issues in the observational study of space debris, and a discrepancy between the RCS and the physical projected area has already been reported for known objects.[3,4]

One of the major advantages of using the MU radar in debris observation is that a simple low-frequency approximation holds for the analysis of scattering of the MU radar signal from most space debris, in contrast to most debris radars for which the relationship between the shape of debris and its RCS is quite complicated. It thus seems to be feasible to extract some information on the debris shape from the MU radar data. Here we try to interpret the RCS variations of space debris observed

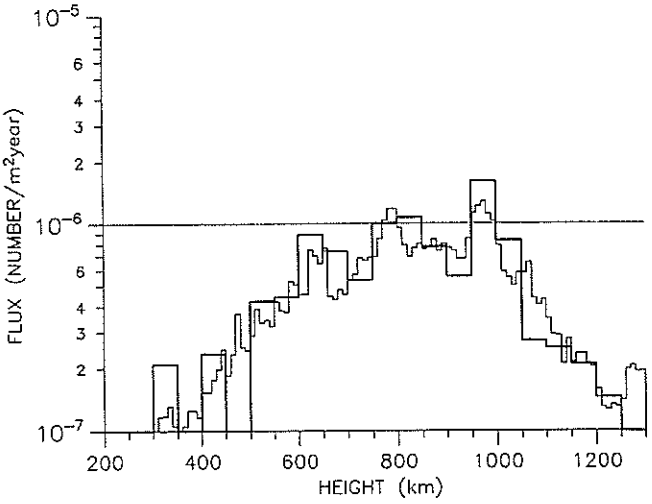

Fig. 1 Height distribution of the debris flux derived from the MU radar observations (thick line) and from the US SPACECOM catalog.

Received March 19, 1993; revision received June 28, 1993; accepted for publication June 29, 1993.

*Associate Professor, Department of Electrical Engineering II.
†Graduate Student, Department of Electrical Engineering II.
‡Graduate Student, Department of Electrical Engineering.
§Professor, Department of Electrical Engineering II.

with the MU radar in terms of the equivalent axial ratio of the target.

Another advantage of the MU radar is in its fast beam steerability. The special observation mode developed for debris observations enabled us to observe RCS variations of space debris with unknown orbital elements for over 10 s for each pass.[5] This observation period is about 10 times longer than that available with other radars with a sharp single beam.

Middle and Upper Atmosphere Radar with Debris Observation Mode

The antenna beam of the MU radar has a one-way half-power width of 3.7 deg, and can be pointed to any desired direction within a coverage of 30 deg from the zenith in a switching time of 10 μs. Therefore, it is possible to observe the passage of an object with multiple beams. We developed a special debris observation mode with which the antenna beam is switched alternately from pulse to pulse among eight directions arranged closely around the zenith.

In the debris mode, eight antenna beams are arranged as shown in Fig. 2, so that objects passing through this region can be observed by at least three overlapping beams simultaneously. The abscissa and the ordinate shows the east-west and the north-south angle from the zenith in degrees. Solid and dashed circles denote the half-power width of the beam and its effective coverage of 3 deg from the center, respectively. Small circles overlayed on Fig. 2 show a path of a radar calibration satellite LCS-4 as determined every 1 s by the method explained earlier. The straight line shows the linear fit to these points with plus symbols indicating the location of the object for every 1 s on the line. This satellite is an aluminum sphere with a diameter of 1.129 m and weight of 34 kg, launched by the Massachusetts Institute of Technology Lincoln Laboratory in 1971.[6] It has a polar circular orbit with an inclination of 87 deg and a height of 800 km.

Accurate instantaneous direction of the object is determined by comparing the echo intensity from different beams, knowing each beam pattern. The antenna beam pattern of the MU radar is precisely computed and is confirmed by various methods such as the reception of the radar signal on a satellite[7] and the observation of the reflection pattern from the moon.[8] Figure 3 presents the computed ratio of the echo power from a target located between two adjacent beams. Dashed curves are circles of 3-deg radius, which indicate the effective coverage of each beam. Although the absolute echo power is subject to slight ambiguities in the output power, antenna system loss, and the receiver gain, the ratio of the echo power from two antenna

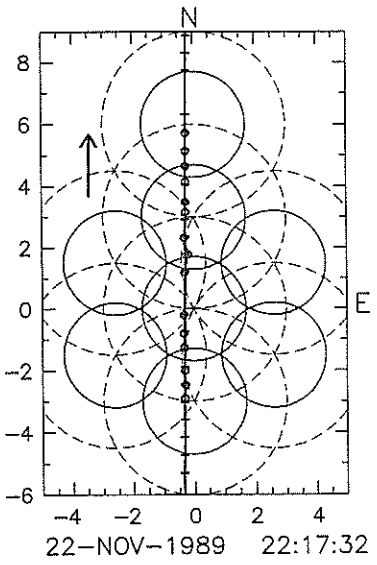

Fig. 2 Beam arrangement of the debris mode and a path of LCS-4 satellite.

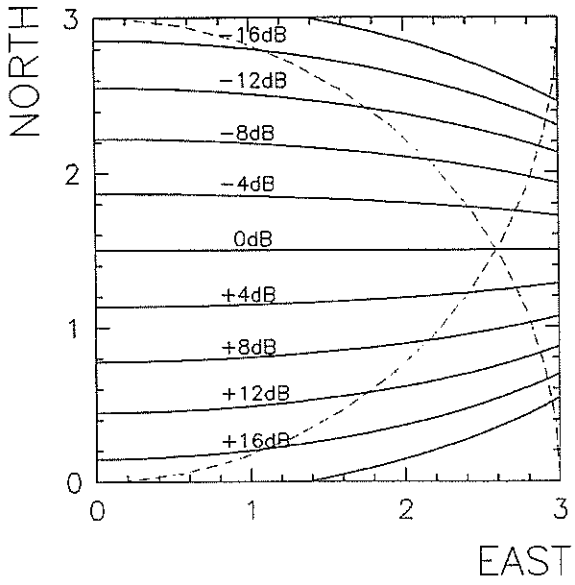

Fig. 3 Computed echo power ratio of a point target located between two adjacent antenna beams separated by 3 deg.

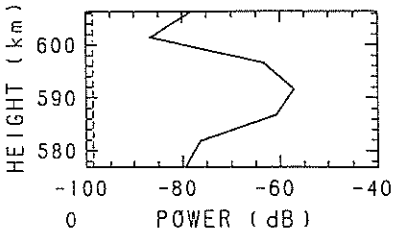

Fig. 4 Measured height pattern of the received echo power after pulse decompression.

beams measured by successive pulses can be determined with an accuracy of the order of 0.1 dB. Once the echo power ratio is measured, we can tell that the target is located on a certain curve as shown in the figure. The exact direction of the target is given as the intersection of two such curves drawn using the echo power ratio from three adjacent beams. It is then possible to compensate for the antenna gain reduction to get the accurate RCS value at each time.

The range also is determined with a much finer resolution than the pulse width using a similar technique. The pulse waveform of the MU radar is controlled carefully using a seven-stage Thomson filter to satisfy the regulation against spurious radiations outside the allocated frequency band for the MU radar. Figure 4 is an example of the measured height pattern. The dashed line on the left indicates the background noise level. The transmitted pulse is coded with a seven-element Barker code with the subpulse width of 64 μs, and the received signal is oversampled at a 32-μs interval. The figure shows the output of the decoder (or a digital correlator) for the pulse compression. The accurate height of the target is computed by fitting the theoretical response of the decoder output signal to the observed pattern.

This technique of multiple beams not only enlarges the search area of a sharp single beam, but also provides RCS variation of unknown objects for a period of 10–20 s compared to a fraction of a second available with other radars with a fixed beam position. Table 1 summarizes the radar parameters of the debris mode.

Figure 5a shows the height of LCS-4 vs time for the same observation as Fig. 2. Circles and plus symbols indicate the height of the satellite directly determined every 1 s and the height after linear fitting of the path, respectively, as shown in Fig. 2. The good fit of each determined point to a straight line shown in Figs. 2 and 5 suggests that the direction and the

Table 1 Observational parameters of the MU radar for the debris mode

Parameter	Value
Location	Shigaraki, Shiga, Japan (34.85°N, 136.10°E)
Radar system	Monostatic pulse radar; active phased array system
Operational frequency	46.5 MHz
Antenna	Circular array of 475 crossed Yagi antennas
Aperture	8330 m² (103 m in diameter)
Beam width	3.6° (one way; half-power for full array)
Steerability	Steering is completed in each IPP
Beam directions	8(3° vertical, and 6° off-zenith) (see Fig. 2)
Polarization	Right-hand circular
Transmitter	475 solid state amplifiers (Transmit/receive modules; each with output power of 2.4 kW peak and 120 W average)
Peak power	1 MW
Average power	45 kW (duty ratio 4.5%)
Pulsewidth	448 μs (64 μs × 7 bit)
Inter pulse period	10 ms
Receiver	
Intermediate frequency	5 MHz
A/D converter	12 bits × 2 channels
Pulse compression	7-element Barker Code
Observed range	201.46 km–810.63 km
Range resolution	9.6 km
Time resolution	1 s

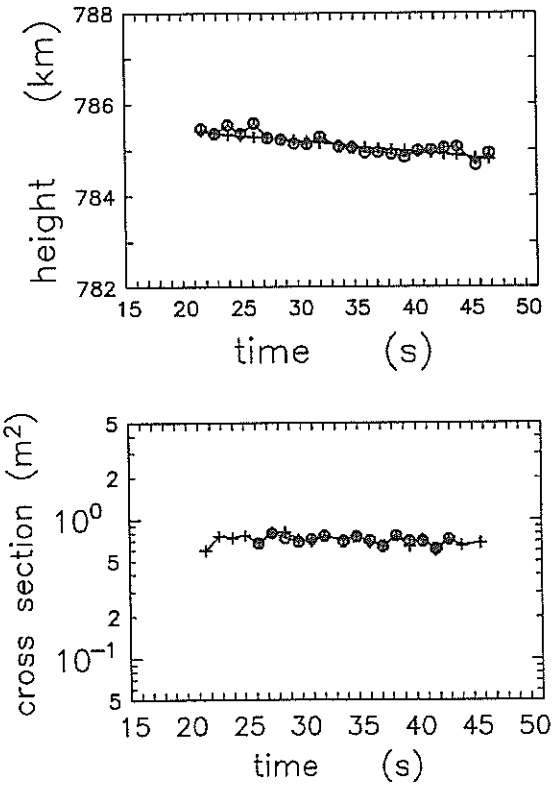

Fig. 5 Variations of LCS-4 satellite vs time: a) height variation and b) RCS variation.

range of the satellite is determined with an accuracy of about 0.1 deg and 200 m, respectively. It should be noted that the beamwidth of 3.7 deg and the range resolution of 9.6 km of the system are several tens of times larger than these values. It is possible to roughly calculate the orbital elements of the satellite from the determined path. The obtained inclination, for example, agrees with the real value within an error of 2 deg.

Figure 5b shows the variation of RCS vs time. Since the radar did not have an accurate absolute calibration, this experiment is used to determine the system constant, and the mean observed RCS value is adjusted to its theoretical value of 0.70 m². The fluctuation of RCS shown in Fig. 5b indicates the magnitude of the random errors in the RCS determination. It is estimated to be 0.4 dB, which gives the lower boundary of RCS variation detectable with the MU radar at this range.

Radar Cross Section Variations

The constant RCS shown in Fig. 5b is a rather exceptional example of a purely spherical object, and most of debris should have some sort of asymmetry as well as spin motion. Thus, it is expected that observations of time variation of RCS will give us information concerning the shape of the object.

Bohannon and Young[9] examined RCS variations of known objects by tracking them using the Haystack X-band radar and reported RCS variations which show very high-frequency components extended to the order of 100 Hz. On the other hand, the RCS variation of the same object observed by the ALCOR C-band radar, which they cited for comparison, shows a similar high-frequency component superimposed on the dominant periodicity of 0.1–1 Hz. It seems that X-band RCS variations mainly exhibit aspect sensitivity typical to objects much larger than the radar wavelength, whereas the lower frequency C-band variations are dominated by the spin motion of the entire body.

Although these observations with high-frequency (here used to mean that the radar wavelength is shorter than the size of the target) radars may provide detailed information of the complexity in the shape of the object, low-frequency (wavelength comparable or larger than the size of the target) observation is suitable in determining the basic shape of the object, such as the axial ratio which is important in estimating the mass of the object from the RCS.

Figure 6 shows an example of the RCS variation of the COSMOS 1023 rocket booster observed by the MU radar. It is a cylindrical body of 7.4 × 2.4 m (maximum optical cross section 17.8 m²). The symbols in the figure have the same meanings as in Figs. 2 and 5. Figure 6 clearly shows a smooth variation of the RCS, probably associated with its rotation. The maximum value of RCS agrees well with the optical cross section. Since this is one of the largest objects in orbit, all debris falls in the size region where the low-frequency approximation holds in computing the RCS. In such a case, the frequency of the dominant component in the RCS variation spectrum gives the spin rate, and its magnitude is related to the axial ratio of the object as discussed in more detail subsequently.

Although the number of observations with this mode is still very limited because of the machine time allocation of the radar, which is designed and operated mainly for the purpose of atmospheric sciences, we have so far made observations over 100 h, and accumulated 133 cases of debris encounter. They are classified into four categories according to the mean RCS value in each observation. The classes are chosen to evenly cover the dynamic range of RCS observed by the MU radar in

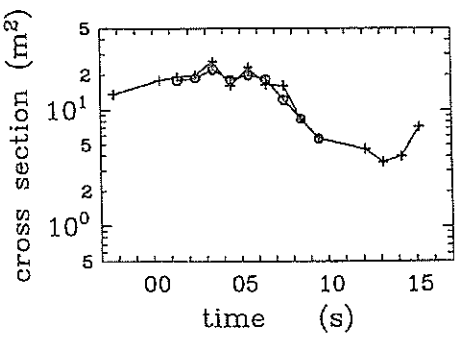

Fig. 6 RCS variation of the COSMOS 1023 rocket booster.

a logarithmic scale. Figure 7 shows the RCS variation spectra for each category. For each observation, which consists of 10–20 samples of RCS taken at a 1-s interval along the path of the object, relative RCS variation around its mean value is first computed on the log-scale. Then its frequency power spectrum is computed and averaged for different observations in each category. The frequency resolution of each figure is about 0.03–0.05 Hz, which is determined by the duration of each observation. Clearly, the spectra are dominated by long-period components around 0.05 Hz, showing that the RCS variations are dominated by those associated with slow spin motions.

The most important feature revealed by this analysis is the tendency that the magnitude of the relative RCS variations, which indicates the axial ratio of the objects, is larger for objects with smaller RCS values. This result suggests that the small objects with RCS of less than 1 m^2 have larger axial ratio, or in other words, more elongated shape than larger objects. A thin rod or a ribbon of length much shorter than the wavelength of 6.4 m should show a large RCS variation because it can be well approximated by an electric Hertz dipole.

Therefore, it is likely that these small objects are lighter than the solid sphere of the same RCS as is usually assumed in evaluating the effect of possible collision with debris.

Model Computation

To quantitatively examine the relation between the observed RCS variations and the effective axial ratio, we made a simple model computation.

Since most space debris falls into the Rayleigh region of scattering (size is approximately not greater than radar wavelength) at the frequency of 46.5 MHz, a low-frequency approximation holds for the MU radar observations of space debris. Here we assume the simplest shape of a perfectly conducting ellipsoid as a target for which an analytical expression is given for the scattering cross section under the low-frequency approximation.[10] It is further assumed that an ellipsoid is rotating around its major principal axis, which coincides with the shortest axis of symmetry for an ellipsoid. This is the most stable state of the spin motion, into which all objects with nonzero internal energy loss fall after a sufficiently long time.

Figure 8 is an example of RCS variation of an ellipsoid computed for different polarizations under the low-frequency approximation. The σ_ϕ and σ_θ denote RCS for linear polarization with the electric field parallel and perpendicular to the major axis, respectively, and σ is for the circular polarization. The right-hand circular polarization is used for the MU radar observations to overcome the problem of Faraday rotation of the polarization plane during the propagation of the radio wave through the ionosphere. Although the reception of the cross (left-hand circular) polarization together with the right-hand one will provide valuable information on the shape of debris, only one polarization can be received with the MU radar system at a time without dividing the antenna area due to a design restriction of the radar system. Thus, only the right-hand circular polarization is considered here.

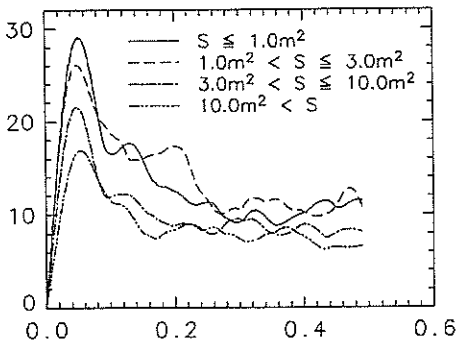

Fig. 7 Frequency power spectra of RCS variations relative to its mean value *S*.

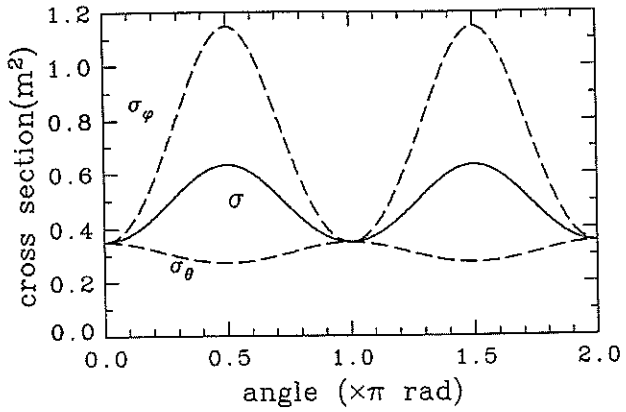

Fig. 8 Example of RCS variation of an ellipsoid vs incident angle of the radar wave.

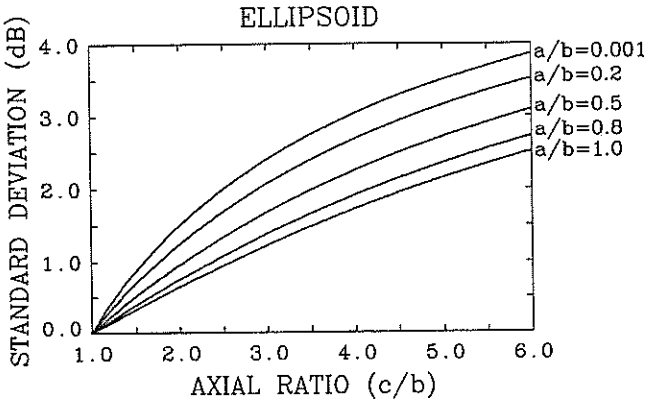

Fig. 9 Computed magnitude of RCS variations of ellipsoids with various shapes.

An important feature found in this figure is that the angular variation shows an almost purely sinusoidal pattern, in contrast to random angular patterns with which we are familiar for objects larger than the radar wavelength.[10,11] The RCS variation shown in Fig. 6 clearly shows a similar sinusoidal pattern. Although the frequency of the sinusoid gives the spin rate of the object, it does not contain much information related to its shape. Since the phase apparently has no meaning for a statistical study, the amplitude is the only parameter that can be related to the shape of the object. It is then reasonable to take the standard deviation of the RCS relative to its mean value as the representative parameter.

The theoretical RCS variation relative to its mean value over one rotational period is computed for an ellipsoid of given axial ratio, and averaged over all observational directions. Figure 9 shows the standard deviation of RCS variations vs its axial ratio. Note that the magnitude of RCS variations relative to its mean value is independent of the absolute size of target as far as the low-frequency approximation holds.

As shown in this figure, the RCS and its variation is a function of not only the major axial ratio (c/b), but also the ratio of minor axes (b/a). We note here that the radiation impedance of a wire antenna of an arbitrary cross-sectional shape is well approximated by a cylindrical antenna whose radius r is given by

$$\log r = \frac{1}{l^2} \oint_C \oint_C \log d(\eta, \xi)\, d\eta\, d\xi \qquad (1)$$

This radius is called the geometrical mean distance (GMD). Equation (1) shows that the scattering property of a wire is determined by its GMD regardless of its cross-sectional shape. This fact implies that the observation of RCS variation provides

only one parameter related to the shape of the target, whereas the physical shape is determined by two parameters. It poses a large limitation in estimating the volume of the target. For example, we can not discriminate a flat ribbon of width w from a cylinder of diameter $w/2$, which has the same cross-sectional GMD as the ribbon, although the former has infinitesimal volume. However, it is still possible to determine the upper limit of the volume of a wire with given GMD, which is obtained by assuming the cross-sectional shape to be a circle of radius r.

Considering this fact, we define "the equivalent axial ratio" of an ellipsoid as c_e/b_e, the ratio of the GMD of two cross sections which contain the axes $c - b$ and $a - b$. Figure 10 is the same as Fig. 9 except that the abscissa is expressed in terms of the equivalent axial ratio. As expected, the magnitude of the RCS variations is characterized by a single parameter c_e/b_e with little dependence on b/a.

Interpretation of Observations

The model computation made in the previous section shows that we can deduce the equivalent axial ratio of the debris assuming they have ellipsoidal shapes. It is further assumed that observations are made from all directions and for over the entire cycle of rotation of the object. Since these assumptions are not satisfied for a single observation of an object, in which the relation between the rotational axis and the direction of observation is not known, we can only make a statistical comparison. Here we interpret the mean RCS variation as shown in Fig. 7 in terms of the equivalent axial ratio, assuming it represents the average shape of all objects in each category of the mean RCS.

Since the RCS of objects smaller than the radar wavelength is mainly determined by its largest dimension, it is expected that the volume of an ellipsoid is smaller than a sphere which has the same mean RCS. Figure 11 shows the volume ratio of the ellipsoid and sphere of equal RCS vs the equivalent axial ratio. This figure indicates the magnitude of overestimate of the volume when the radar echo from an ellipsoidal debris is interpreted assuming a spherical shape, as is the case for most of the studies which refer to US SPACECOM catalog data. For example, if the equivalent axial ratio of a target is 3, it has at most half of the volume of a sphere of the same mean RCS. The degree of overestimate is even larger if it has a flat cross section (small a/b value).

Table 2 lists the number of data, the equivalent axial ratio, and the maximum volume ratio obtained from Fig. 7 for each class of RCS. Since the equivalent axial ratio is in the range of 2–3, the volume, and hence the mass, of the debris is estimated to be 40–70% of a sphere of the same RCS. The standard deviation of the mean standard deviation of RCS in each class is 0.4–0.6 dB. The error bar of the equivalent axial ratio and the maximum volume ratio is thus estimated to be about 0.5

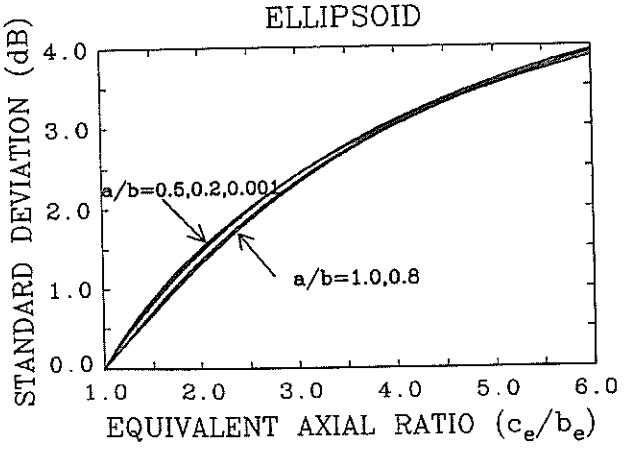

Fig. 10 Computed magnitude of RCS variations vs the equivalent axial ratio c_e/b_e.

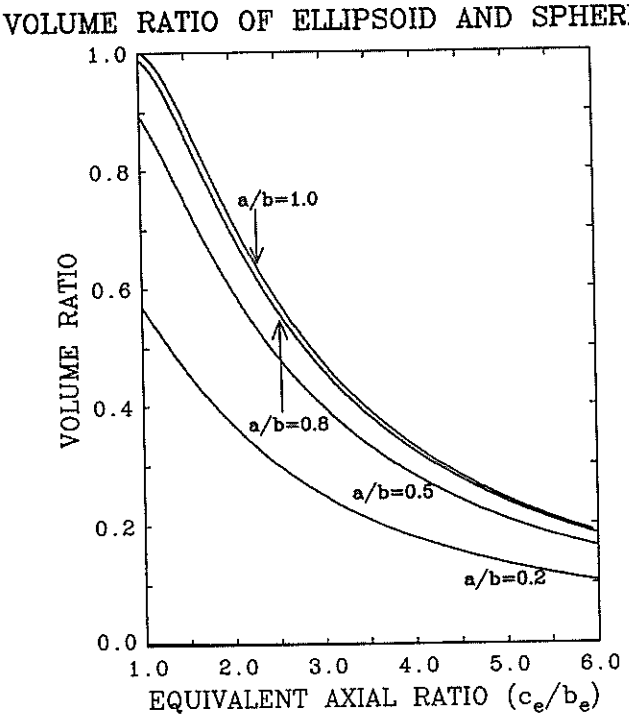

Fig. 11 Volume ratio of an ellipsoid and sphere of equal mean RCS.

Table 2 Statistics of debris for different RCS classes

Mean RCS, m²	Cases	c_e/b_e	Max. volume ratio
$S < 1.0$	33	3.02	0.471
$1.0 < S < 3.0$	21	3.22	0.435
$3.0 < S < 10.0$	55	2.34	0.620
$10.0 < S$	24	2.08	0.692

and 0.1, respectively. As discussed in the previous section, the real volume ratio should range from 0 to these maximum values depending on the unknown cross-sectional shape in the plane perpendicular to the longest axis of each object. If we take $a/b = 0.5$ as a crude estimate, for example, then for the small objects with RCS of less than 1 m², for which c_e/b_e is estimated as 3.02, the volume ratio becomes 39% of a sphere with equal RCS. The physical axial ratio c/b is 4.25 for this case.

Badhwar and Anz-Meador[4] compared the mean RCS of known objects with their average projected surface area A_{eff}, which is given by

$$A_{\text{eff}} = \frac{1}{4\pi} \int_{\Omega} A(\theta, \phi) \sin\theta \, d\theta \, d\phi \tag{2}$$

and obtained a regression formula of

$$A_{\text{eff}} = 0.571 \ \text{RCS}^{0.767 \pm .048} \tag{3}$$

For an ellipsoid, Eq. (2) reduces to

$$A_{\text{eff}} = \left\{ b^2 + \frac{bc^2 \arccos(b/c)}{\sqrt{c^2 - b^2}} \right\} E(\sqrt{1 - b^2/a^2}) \tag{4}$$

By substituting the parameters just given, we obtain from Eq. (4) that $A_{\text{eff}} = 0.765\text{RCS}$ for the range of RCS < 1 m². The average of $A_{\text{eff}}/\text{RCS}$ in Eq. (3) for the same range is 0.744, which is in very good agreement with our value. However, we should be careful in comparing our result with that of Badhwar and Anz-Meador, since their RCS values are measured by the Eglin uhf radar, whose wavelength is 68 cm. Thus objects with

RCS of 1 m^2 are out of the Rayleigh region of scattering. The angular pattern of the RCS of an ellipsoid becomes more specular as the size becomes larger, with an enhanced peak at the normal incidence of the radio wave to the major axis.[10] Although no theoretical expression such as Eq. (4) is available in this region, it is expected that the deviation of the shape from ellipsoid gives more variability than in the Rayleigh region. We should thus consider the cited agreement only as an indication of consistency.

Our major limitation in the present study is the sensitivity for small objects, which could only be resolved by employing a higher frequency. If we are to extend our approach to the size region of 1–10 cm for which we have the least amount of information, a frequency around 3 GHz will be appropriate so that we can still apply the low-frequency approximation. As we have seen, the multiple-beam capability is essential in studying the RCS variation of unknown targets. To obtain larger angular coverage, the sensitivity should be achieved mainly by a higher output power rather than a larger antenna aperture. An example of the system parameters for such a radar is: frequency 3 GHz, peak output power 300 kW, pulse width 16-μs $\times$ 64-bit compression, and antenna area 300 m^2 (beamwidth 0.3 deg). This system can detect a sphere of 1 cm diam at the range of 500 km. If we switch 100 beam directions with an interpulse period of 10 ms, we can cover an angular region of about 3 deg from the zenith by the method described here. Although it would be an expensive system because it requires an active phased array consisting of 10,000 elements of 30 W amplifier, it would serve as a complementary sensor to the sensitive radars with a sharp single beam, such as the Haystack X-band radar or the Near Earth Assessment Radar.

Summary

We have compared the observations of RCS variations made by the MU radar with a model calculation to derive information on the shape of debris. At a frequency of 46.5 MHz, which is used by the MU radar, most debris falls into the Rayleigh region of scattering, in which the variation of RCS is dominated by a sinusoidal component associated with the rotation of debris.

We then tried to interpret observed RCS variations in terms of the axial ratio of the objects assuming they have ellipsoidal shapes. It was found that only a single parameter, which we defined as the effective axial ratio, can be derived from RCS variations of an object in the Rayleigh region.

The comparison of observations and the model computation showed that the volume of small objects with the mean RCS of less than 1 m^2 seem to be, at most, half that of spheres having the same RCS. The result of the model computation was also consistent with the relation of A_{eff} and RCS estimated for known objects.

Acknowledgment

The authors wish to thank the staff members of Radio Atmospheric Science Center, Kyoto University for their support for the observations. The MU radar belongs to and is operated by Radio Atmospheric Science Center, Kyoto University. They are grateful to Anthea Coster and her colleagues of MIT Lincoln Laboratory for providing the information on LCS-4 satellite, and also to Andrew Potter of NASA Johnson Space Center and Phillip Anz-Meador of Lockheed Engineering and Sciences Co. for their help in identifying the Cosmos 1023 rocket booster.

References

[1] Kessler, D. J., "Orbital Debris Environment for Spacecraft in Low Earth Orbit," *Journal of Spacecraft and Rockets*, Vol. 28, 1991, pp. 347–351.

[2] Sato, T., Kayama, H., Furusawa, A., and Kimura, I., "MU Radar Measurements of Orbital Debris," *Journal of Spacecraft and Rockets*, Vol. 28, 1991, pp. 677–682.

[3] Badhwar, G. D., Potter, A. D., Anz-Meador, P. D., and Reynolds, R. C., "Characteristics of Satellite Breakups from Radar Cross Section and Plane Change Angle," *Journal of Spacecraft and Rockets*, Vol. 25, 1988, pp. 420–426.

[4] Badhwar, G. D., and Anz-Meador, P. D., "Determination of the Area and Mass Distribution of Orbital Debris Fragments," *Earth, Moon, and Planets*, Vol. 45, April 1989, pp. 29–51.

[5] Sato, T., Kayama, H., Furusawa, A., and Kimura, I., "MU Radar Observations of Space Debris," *Advances in Astronautical Sciences*, Vol. 77, 1992, pp. 273–282; also AAS Paper 91-636.

[6] Prosser, R. T., "The Lincoln Calibration Sphere," *Proceedings of the Institute of Electrical and Electronics Engineers*, Vol. 53, Oct. 1965, pp. 1672–1676.

[7] Sato, T., Inooka, Y., Fukao, S., and Kato, S., "Multi-Beam Pattern Measurement of the MU Radar Antenna by Satellite OHZORA," *Journal of Geomagetism and Geoelectricity*, Vol. 41, Sept. 1989, pp. 743–751.

[8] Fukao, S., Sato, T., Tsuda, T., Yamamoto, M., Yamanaka, M. D., and Kato, S., "MU Radar: New Capabilities and System Calibrations," *Radio Science*, Vol. 25, July/Aug. 1990, pp. 477–485.

[9] Bohannon, G. E., and Young, N. A., "Verification and Validation of Algorithms for Obtaining Debris Data using High Frequency Radars," AIAA Paper 90-3869, Jan. 1990.

[10] Ruck, G. T. (ed.), *Radar Cross Section Handbook*, Vol. 1, Plenum Press, New York, 1970, pp. 341–376.

[11] Skolnik, M. I. (ed.), *Radar Handbook*, McGraw-Hill, New York, 1990, pp. 11.1–11.18.

Alfred L. Vampola
Associate Editor